First-principles study on 3*d* transition-metal dihydrides

Kazutoshi Miwa and Atsuo Fukumoto
Toyota Central Research & Development Laboratories, Inc., Nagakute, Aichi 480-1192, Japan
(Received 19 November 2001; published 1 April 2002)

The ultrasoft pseudopotential calculations are performed for the CaF_2-type dihydrides TiH_2, VH_2, and CrH_2. The calculated lattice constants agree well with the experimental data except for CrH_2. We also perform calculations for a solution of hydrogen in Fe and Ni and obtain the site preferences correctly. The results for the heats of formation and heats of solution show that the calculations give the correct trends for exothermic through endothermic reactions but overbind hydrogen with transition metals, typically about 20 kJ/mol H_2. This overbinding is improved by including the zero-point energy correction. The energetics of binary dihydrides including hypothetical FeH_2 and NiH_2 is discussed in term of three contributions: namely, the structural transformation energy, the lattice expansion energy, and the hydrogen insertion energy. The former two contributions are understood from the nature of the host metals. The hydrogen insertion energy can be represented by a simple geometric model. The extension of this model is also suitable for alloy dihydrides.

DOI: 10.1103/PhysRevB.65.155114 PACS number(s): 71.20.Be, 81.05.Je, 71.15.Mb

I. INTRODUCTION

The heat of formation is the most fundamental and important quantity for hydrides, in particular, considering application to hydrogen storage systems. It is crucial to control the heat of formation for designing hydrogen storage materials, on which the condition for hydrogenation and dehydrogenation depends strongly. Several models[1–5] have been proposed for the heat of formation (solution). Semiempirical approaches such as the embedded-atom model[6] have been applied successfully for the metal-hydrogen systems.[7,8] First-principles calculations have been also utilized to study various properties,[9–14] but a theoretical prediction of the heat of formation is still rare.[9,13]

In this work, we study the 3*d* transition-metal dihydrides in the CaF_2-type structure using first-principles calculations. The first-row transition metals are favorable in applications because of their relative low densities. The CaF_2-type dihydride is commonly observed for the early transition metals and their alloys and is an important class of hydrogen storage alloys, such as a Ti-V-Cr alloy.[15] One of our purposes is to examine the accuracy of the theoretical prediction. To this end, the solution of hydrogen in Fe and Ni is considered as examples of endothermic reactions, in addition to the dihydrides TiH_2, VH_2, and CrH_2. The other purpose is to understand the energetics of dihydride formation. Hydrogenation affects the host metal lattice and induces various effects such as lattice expansion and structural transformation, which are not taken into account in the early models.[1–3] These contributions to the heat of formation are not clear. Therefore, we decompose the heat of formation into the contribution of the lattice deformation and that of the hydrogen-metal interaction, and discuss them separately.

The rest of this paper is organized as follows: In Sec. II, our theoretical approach is described. Section III presents the results, and the discussions of the results are given in Sec. IV. Section V summarizes the main results of this study. We use units of kJ/mol H_2 for the energies related to hydrogenation, where 1 eV/H_2 = 96.48 kJ/mol H_2.

II. METHOD

The present calculations have been performed using the ultrasoft pseudopotential method[16] based on density functional theory.[17] The generalized gradient approximation (GGA) proposed by Perdew, Burke, and Ernzerhof[18] is used for the exchange-correlation energy.

All pseudopotentials are constructed from the results of scalar-relativistic all-electron calculations.[19] The pseudo wave functions and the pseudoaugmentation charge functions are optimized by a method similar to that proposed by Rappe *et al.*[20] The hydrogen pseudopotential is constructed for 1*s* and 2*p* states, where a single-projector function is employed for each angular momentum component. For transition-metal atoms, 3*d*,4*s*, and 4*p* states are chosen as reference states. We use double-projector functions for the *d* component and a single-projector function for the *s* and *p* components. The partial core correction[21] is adopted to enhance the transferability of the pseudopotentials. For Ti, V, and Cr, pseudopotentials including 3*s* and 3*p* states as valence are also generated in order to check the effects of the shallow semicore states. In this setup, the *s*, *p*, and *d* components are treated with double-projector functions. We will refer to these pseudopotentials as the *sc* pseudopotentials. As shown latter, the semicore states have only minor effects for the hydrides studied here, and so we will present the results obtained using the frozen-semicore pseudopotentials otherwise noted.

In solid-state calculations, the Kohn-Sham equation is solved by the iterative diagonalization scheme[22] and the Broyden charge mixing method[23] is adopted to accelerate the convergence. The macroscopic stress tensor and the atomic forces are utilized for structural optimization.[24] During the optimization process, the partial occupation numbers near the Fermi level are determined by the Fermi-Dirac distribution function with $k_BT = 3\times10^{-3}$ hartree and the free-energy functional[25] is minimized instead of the Kohn-Sham energy functional. Then, the Kohn-Sham energy functional is minimized with the improved tetrahedron method[26] at the optimized structure. The heat of formation is obtained by sub-

TABLE I. Lattice constants a and c (Å) and cohesive energy E_{coh} (eV) of bulk transition metals. The results obtained using the pseudopotential including the semicore states are labeled *sc*. For Cr, the commensurate antiferromagnetic structure is assumed. For Fe and Ni, the ferromagnetic structure is taken into account.

	Structure	a	c	E_{coh}	
Ti	hcp	2.956	4.689	5.98	Present
		2.950	4.657	5.92	Present(*sc*)
		2.95	4.68	4.85	Expt.[a]
V	bcc	3.014	—	6.65	Present
		2.997	—	6.53	Present(*sc*)
		3.03	—	5.31	Expt.[a]
Cr	bcc	2.878	—	4.03	Present
		2.872	—	4.03	Present(*sc*)
		2.88	—	4.10	Expt.[a]
Fe	bcc	2.851	—	5.40	Present
		2.87	—	4.28	Expt.[a]
Ni	fcc	3.524	—	6.25	Present
		3.52	—	4.44	Expt.[a]

[a]Reference 27.

tracting the total energies of the bulk metal and the molecular hydrogen from that of the metal hydride.

The pseudo wave functions are expanded by plane waves with a cutoff energy equal to 15 hartrees. The cutoff energy for the charge density and potential is set to be 120 hartrees. The number of k sampling points is described in the following sections. The errors of the heat of formation (and solution) caused by the finite cutoff energy and k sampling points are estimated to be less than 1 kJ/mol H_2.

III. RESULTS

The results of the lattice constants and the cohesive energy for the bulk transition metals are shown in Table I, including those obtained using the *sc* pseudopotentials. For Cr, which is an incommensurate antiferromagnet in the ground state, the commensurate antiferromagnetic structure has been assumed by doubling the unit cell. For Fe and Ni, the ferromagnetic structure has been taken into account. We have employed a $12\times12\times8$ k-point grid for Ti, $10\times10\times10$ grid for Cr, and $12\times12\times12$ grids for the others. The calculated lattice constants agree very well with the experimental values. The spin magnetic moments are obtained as $2.25\mu_B$ and $0.62\mu_B$ for Fe and Ni, respectively. These are also in good agreement with the experimental values[27] ($2.22\mu_B$ for Fe and $0.61\mu_B$ for Ni). The cohesive energies are overestimated except for Cr.

The calculation for the molecular hydrogen has been performed using a cubic supercell with size of $6\times6\times6$ Å^3. The bond length is predicted as 0.768 Å and the binding energy as 432 kJ/mol H_2. The agreement with the experimental data (0.741 Å and 456 kJ/mol H_2) is fairly good.

Table II shows the results of the lattice constants and the heats of formation for the CaF_2-type transition-metal dihydrides. The results obtained using the *sc* pseudopotentials are also indicated. For k-point sampling, $10\times10\times10$ grids have been used. For TiH_2, the tetragonal structure is found correctly though the tetragonal distortion is somewhat smaller than the experimental data. The heat of formation is predicted as -145 kJ/mol H_2, which is about 20 kJ/mol H_2 lower than the experimental value. The accurate *sc* pseudopotential gives almost identical results. The origin of the cubic-to-tetragonal distortion is thought to be a Jahn-Teller effect. In Figs. 1(a) and 1(b), we plot the energy dispersion curves of TiH_2 in the cubic and tetragonal phases, respectively. In the cubic phase, a doubly degenerate flat branch across the Fermi level is observed. The tetragonal distortion lifts the degeneracy of this branch and makes the one fully occupied and the other almost unoccupied. The underestimation of the tetragonal distortion might be attributed to using the Fermi-Dirac function with moderate temperature during the structural optimization process, which reduces the energy

TABLE II. Lattice constants a and c (Å) and heats of formation, ΔH(kJ/mol H_2), of CaF_2-type transition-metal dihydrides. The results obtained using the pseudopotentials including the semicore states are labeled *sc*.

	Structure	a	c	ΔH	
TiH_2	Tetra.	4.486	4.352	-145	Present
		4.480	4.347	-142	Present(*sc*)
		4.53	4.28	-124	Expt.[a]
VH_2	Cubic	4.234	—	-65	Present
		4.223	—	-61	Present(*sc*)
		4.27	—	-40	Expt.[a]
CrH_2	Cubic	4.103	—	17	Present
		4.101	—	19	Present(*sc*)
		3.86	—		Expt.[b]

[a]Reference 28.
[b]Reference 29.

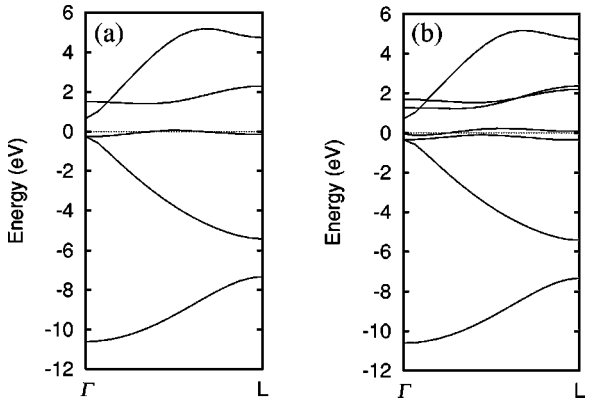

FIG. 1. Energy dispersion curves of TiH_2 in the (a) cubic phase and (b) tetragonal phase. The curves are plotted in the Γ-L direction of the fcc Brillouin zone for the cubic phase and the corresponding direction in the fct Brillouin zone for the tetragonal phase. The origin of the energy is set to be the Fermi level.

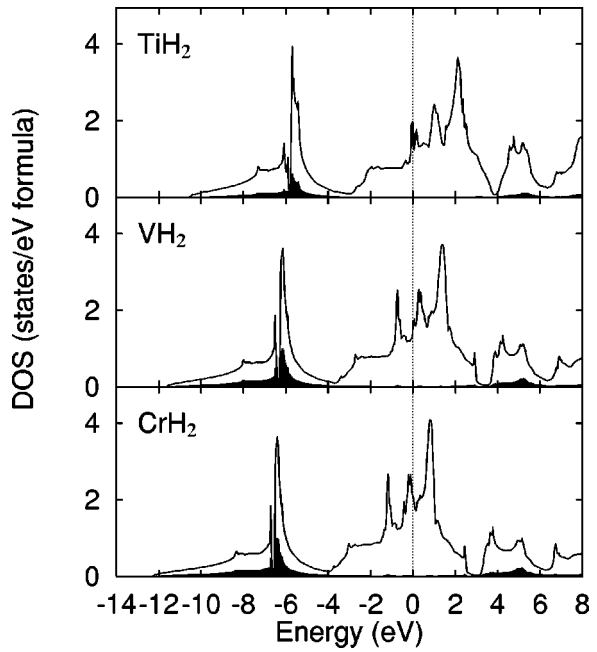

FIG. 2. Density of states for CaF_2-type transition-metal dihydrides. The shaded parts indicate the partial density of states of hydrogen atoms. The origin of the energy is set to be the Fermi level.

gain of the Jahn-Teller distortion. Because the contribution of the tetragonal distortion to the heat of formation is below 1 kJ/mol H_2 in our calculation, we can expect that this contribution is less important for the energetics of hydride formation.

For VH_2, the calculated lattice constant agrees well with the experimental value. The heat of formation is obtained as -65 kJ/mol H_2, which is 25 kJ/mol H_2 lower than the experimental data. The results of the *sc* pseudopotential are almost same. We confirm the stability of the cubic phase by applying the tetragonal and trigonal distortions to it. For CrH_2, there is remarkable difference between the predicted lattice constant and the measured one. The heat of formation is predicted as 17 kJ/mol H_2. To our knowledge, no experimental data have been published for CrH_2. Using the *sc* pseudopotential, the results are hardly changed and the discrepancy found for the lattice constant is not improved. The reason for this discrepancy is uncertain. In this connection, the discussion will be presented in the next section. The stability of the cubic phase is proved by the same way as the case of VH_2.

Figure 2 depicts the density of states (DOS) for TiH_2, VH_2, and CrH_2. These are well described in a rigid band model. The states at the Fermi level consist of the metal *d* states and the relative positions of these states shift lower energies as increasing the number of valence electrons. The hydrogen-induced states are observed below the metal *d* states as the double-peaked shapes.

The heats of solution of hydrogen in Fe and Ni have been calculated using supercells containing 16 metal atoms. We employ $6\times6\times6$ *k*-point grids. The lattice constants are fixed at the theoretical values of the bulk metals and the atomic positions are only allowed to relax. For both Fe and Ni, we consider two hydrogen positions, the tetrahedral (*T*) and octahedral (*O*) interstices. The results are summarized in Table III. For Fe, the heat of solution for the *T*-site occupation is lower than that for the *O*-site occupation, which is consistent with the fact that the observed hydrogen position is *T* site. The heat of solution obtained for *T*-site occupation is 36 kJ/mol H_2, which is 22 kJ/mol H_2 lower than the measured value. For Ni, it is also predicted correctly that the *O*-site occupation which is observed experimentally has lower heat of solution than the *T*-site occupation. The calculated value for the *O*-site occupation, 22 kJ/mol H_2, is 10 kJ/mol H_2 smaller than the experimental one. In order to check the effect of the supercell size, we repeat calculations using the supercell containing 32 metal atoms for the *O*-site occupation in Fe, for which the size effect is expected to be emphasized because the local uniaxial strain is considerably introduced by a H atom. Using the larger supercell, the heat of solution is lowered by 6 kJ/mol H_2. In the cases of the occupation observed experimentally, the effect of the supercell size is probably more smaller, because of the small local strain introduced by H.

TABLE III. Heats of solution of hydrogen in Fe and Ni, ΔH_∞(kJ/mol H_2) and the interatomic distance between hydrogen and surrounding metal atoms, $d_{\text{H-}M}$ (Å). The value in parentheses shows the deviation from the unrelaxed geometry.

	Site	ΔH_∞	$d_{\text{H-}M}$	
Fe	*T*	36	1.660 (4%)	Present
	O	70	1.567 (10%), 2.010 (0%)	Present
	T	58		Expt.[a]
Ni	*T*	73	1.609 (5%)	Present
	O	22	1.796 (2%)	Present
	O	32		Expt.[a]

[a]Reference 28.

IV. DISCUSSION

A. Accuracy

Overall, the theoretical prediction gives correct trends of hydrogenation for exothermic through endothermic reactions. The calculations overbind hydrogen with transition metals, typically about 20 kJ/mol H_2. The large errors found for the cohesive energies of the bulk metals, which are of the order of 100 kJ/mol, do not affect the heats of hydrogenation strongly. This will be due to the fact that a large part of the errors comes from the atomic calculations. In this study, the atomic energies have been calculated for the experimental ground-state configurations, where spherical symmetry was assumed using partial occupation numbers. The cohesive energies, or atomic reference energies, may be improved by lifting this symmetry restriction.[31]

The underestimation for the binding energy of H_2 molecule may be another source of errors. The core radius of the H pseudopotential has been chosen as $r_c=0.56$ Å, which is somewhat large to treat the short bond length of H_2. To

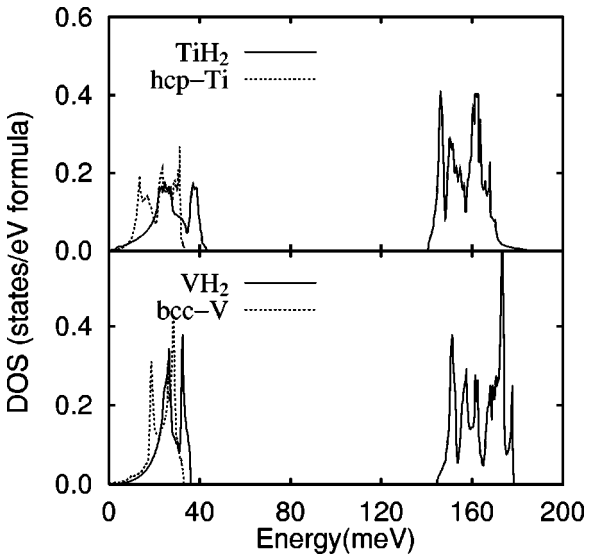

FIG. 3. Phonon density of states for bulk metals and CaF_2-type dihydrides.

check this problem, we repeat calculations using the harder H pseudopotential of $r_c = 0.39$ Å with the large cutoff energy of 50 hartrees. The bond length of H_2 is improved as 0.750 Å and the binding energy as 440 kJ/mol H_2. However, the heat of formation is obtained as -63 kJ/mol H_2 for VH_2 and no improvement is attained.

The overbinding for the hydrogenation of $3d$ transition metals is thought to be intrinsic nature of the calculations. Note that the sign of errors for the heat of formation depends on the bonding character of hydrides: For MgH_2, we have found the underbinding of 20 kJ/mol H_2.

B. Zero-point energy

In first-principles calculations, the ions are treated as classical particles and quantum mechanical effects are ignored. Because of the light mass of hydrogen, the magnitude of the zero-point energy becomes comparable with the results of the heats of formation (solution). In order to estimate this effect, we calculate the zero-point energy correction within the harmonic approximation for the cases where the experimental data of the heats of formation (solution) are available.

For TiH_2 and VH_2, the contribution of both the metal and hydrogen atoms are taken into account. The phonon DOS is calculated by the force-constant method[32] using supercells containing 54 and 32 metal atoms for the bulk metals and dihydrides, respectively. The atomic displacement is chosen to be 0.02 Å. The results of phonon DOS are shown in Fig. 3. For both TiH_2 and VH_2, the hydrogen vibrational states are located around 0.16 eV and separated well from the metal states. The contribution of the low-energy metal states is expected to be small. The zero-point energies obtained from these DOS as well as the corrected heats of formation are summarized in Table IV, where the calculated value of 0.27 eV is used for the zero-point energy of the H_2 molecule. The heats of formation are improved by the zero-energy correction and the agreement with the experimental data becomes very good.

TABLE IV. Heats of formation of CaF_2-type dihydrides including zero-point energy correction. The zero point energies of the host metals, $E^M_{\rm zero}$, and those of the dihydrides, $E^{MH_2}_{\rm zero}$, are given in eV and the heats of formation, $\Delta H_{\rm corr}$, in kJ/mol H_2. The calculated value of 0.27 eV is used for the zero-point energy of H_2 molecule.

	$E^M_{\rm zero}$	$E^{MH_2}_{\rm zero}$	$\Delta H_{\rm corr}$
TiH_2	0.03	0.51	-125
VH_2	0.04	0.53	-43

For the solution of hydrogen in Fe and Ni, we assume that the masses of the metal atoms are infinitely large and these are immobile (the vibration of H in the fixed metal lattice is considered). Supercells containing 16 metal atoms which are fixed at the optimized positions are used. The zero-point energy of hydrogen at the T site in Fe is estimated as 0.24 eV which is in good agreement with the values obtained from the the quantum mechanical calculations,[33] 240 ± 24 meV. The heat of solution is improved considerably as 57 kJ/mol H_2. For hydrogen at the O site in Ni, the zero-point energy and the corrected heat of solution are obtained as 0.15 eV and 25 kJ/mol H_2, respectively. The agreement with the experimental value becomes better.

Although the the zero-point energy correction is important for the quantitative prediction,[34] we expect that this correction has only a small influence on the difference of the heats of formation between the CaF_2-type dihydrides considered here. Therefore, we discuss the energetics of the dihydride formation ignoring the the zero-point energy correction in the following.

C. Energetics of binary transition-metal dihydrides

We decompose the heats of formation of the CaF_2-type transition-metal dihydrides into three contributions: (i) the structural transformation of each host metal to a nonmagnetic fcc structure, (ii) the lattice expansion of the host metal in the fcc structure from its equilibrium spacing to that of dihydride, and (iii) the insertion of hydrogen atoms into the expanded fcc metal. The former two contributions indicate the deformation of the host metals and are determined mainly from the nature of the metals, where the effects of the hydrogen-metal interaction appear implicitly through the amount of lattice expansion. The hydrogen-metal interaction reflects the last contribution. The results of energy decomposition are shown in Fig. 4, where we include hypothetical FeH_2 and NiH_2 to examine the chemical trends along the $3d$ series in the periodic table. The heats of formation are predicted as 69 and 16 kJ/mol H_2 for FeH_2 and NiH_2, respectively. The structural transformation energy of Ti is small because of the similarity between the hcp and fcc structures. For Ni, this energy cost is due to the elimination of the ferromagnetic structure and also small. The other metals have bcc structure, for which the contribution of the structural transformation energy is moderate.

The lattice expansion energy increases with increasing the atomic number until Fe and decreases for Ni. This trend can be understood from the d-band filling. Considering the

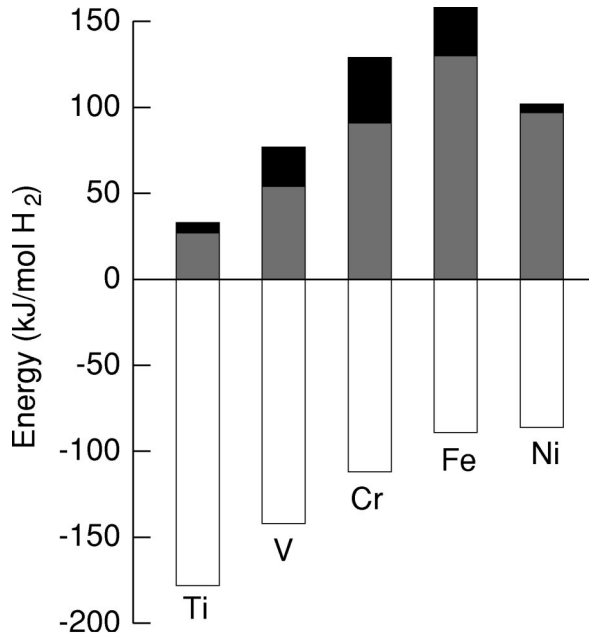

FIG. 4. Decomposed energies for formation of CaF_2-type transition-metal dihydrides. The black, gray, and white parts indicate the structural transformation energy, the lattice expansion energy, and the hydrogen insertion energy, respectively.

simple model proposed by Friedel,[35] transition metals have the maximum in cohesion at the center of the transition-metal series, where the *d* bands are half-filled. Hence, the energy cost for lattice expansion also becomes maximum in the middle of the 3*d* series. The calculated lattice constants and bulk moduli of the metals in the nonmagnetic fcc structure are plotted in Fig. 5. This plot supports the above consideration.

The remaining contribution is the hydrogen insertion energy. We have found that this contribution can be described by a simple geometric model. Figure 6 shows the hydrogen insertion energy E_I as a function of the hydrogen-metal interatomic distance R. The points represent the calculated values, where the left (right) end point for each element corresponds to the equilibrium lattice spacing without (with) hydrogen atoms. The tetragonal distortion of TiH_2 is neglected for simplicity. The relation between E_I and R can be approximately represented by a single curve, regardless of the host metals. This indicates that the hydrogen-metal interatomic distance, or interstitial hole size, is a dominant factor for the hydrogen insertion energy. According to Griessen,[4] the calculated points are fitted to the following analytic function:

$$E_I = \alpha R^{-n} - \beta. \tag{1}$$

When E_I is expressed in kJ/mol H_2 and R in Å, we get the parameters as $\alpha = 1.393 \times 10^4$, $\beta = 2.680 \times 10^2$, and $n = 7.723$ with a root-mean-square deviation of 7.4 kJ/mol H_2. This function is shown as the solid curve in Fig. 6. The value of power n is about 2 times larger than that suggested by Griessen for the heat of solution at infinite dilution. The main reason is most likely due to the hydrogen-

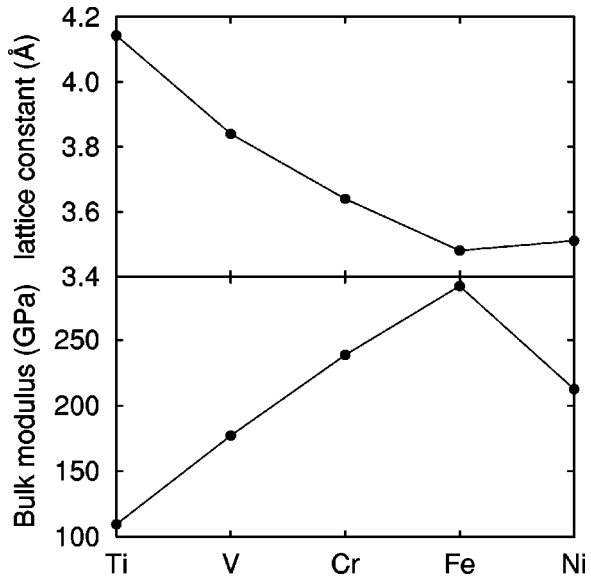

FIG. 5. Lattice constant and bulk modulus of 3*d* transition metals in the nonmagnetic fcc structure.

hydrogen interaction in the CaF_2-type dihydrides, which is also an important factor and is implicitly evaluated from R in Eq. (1). Therefore, the applicability of Eq. (1) will be restricted in this type of dihydrides.

The hydrogen insertion energies are negative for all metals considered here. The heats of formation are determined by the cancellation between this energy gain and the energy cost for the lattice deformation (the structural transformation and the lattice expansion). From Ti to Fe, the variation of both contributions is apparent: The energy gain decreases and the cost increases, so that the heats of formation vary monotonically from strongly negative to positive. For Ni, the energy gain is almost the same as Fe but the cost for the

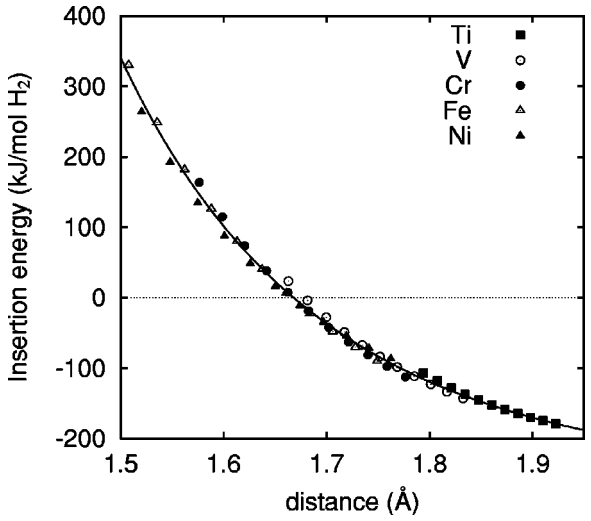

FIG. 6. Hydrogen insertion energy for CaF_2-type transition-metal dihydrides as a function of hydrogen-metal interatomic distance. Points represent the calculated values, where the tetragonal distortion is neglected for TiH_2. The solid curve shows the result of fitting (see in the text).

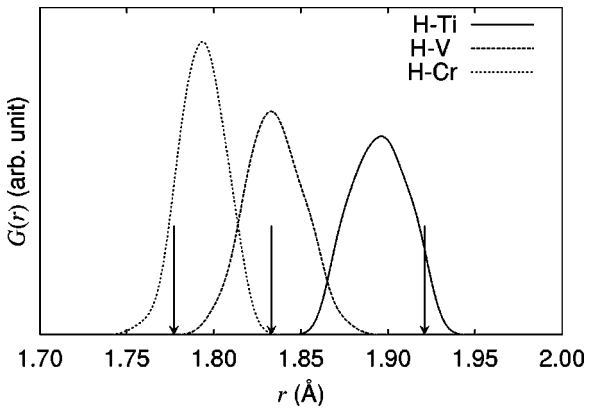

FIG. 7. Partial radial distribution functions of $Ti_6V_{10}Cr_8H_{48}$. The Gaussian broadening with a width of 0.01 Å is used. The arrows indicate the hydrogen-metal interatomic distances of cubic binary dihydrides TiH_2, VH_2, and CrH_2.

lattice deformation becomes small. This is responsible for the small positive formation energy of NiH_2. The similar analysis for the $4d$ transition-metal hydrides will be interesting because of the exothermic reaction between Pd and H, which is the noble exception in the late transition metals.

D. Application to alloy dihydrides

For alloys, Eq. (1) must be modified to describe the local environment dependence. The most straightforward extension is the following form:

$$E_I=\frac{\alpha}{4N_{\mathrm{H}}}\sum_{j=1}^{4N_{\mathrm{H}}}R_j^{-n}-\beta, \tag{2}$$

where N_{H} is the number of H atoms and j runs over H atoms and their nearest-neighbor metal atoms. In order to evaluate the applicability of this, we consider the CaF_2-type dihydride of a Ti-V-Cr alloy. The composition is set to be $Ti_6V_{10}Cr_8H_{48}$ and a supercell containing 24 metal atoms is used. The ordering of the metal atoms assumes it to be random and is determined by means of special quasirandom structures.[36] Hydrogen atoms are placed in all T interstices of the fcc metal lattice. The structural optimization is fully performed for the cell shape and the atomic positions. The average lattice constant calculated from the optimized cell volume is 4.239 Å. The interatomic distances between hydrogen and metal atoms are close to those of binary dihydrides, but vary in a range of about 0.1 Å, as shown in Fig. 7.

From Eq. (2), the hydrogen insertion energy is predicted as -139 kJ/mol H_2. This value agrees very well with -142 kJ/mol H_2 which is obtained from the additional total energy calculation for the supercell removing H atoms. The extended form of Eq. (2) is suitable for alloy dihydrides. In practical applications, it may be convenient to add the correction term $\Delta\beta\simeq 20$ to Eqs. (1) and (2) in order to remedy the overbinding nature of the calculations.

E. Chromium hydrides

The deviation of the calculated lattice constant from the measured one for CrH_2 is 6%, which is considerably larger than the errors of typical GGA calculations. To examine the accuracy of our calculations for the Cr-H system, we perform calculations for CrH in the anti-NiAs structure. As shown in Table V, the calculated lattice constants are fairly good agreement with the experimental data. In Ref. 29, CrH_2 was detected as the cubic hydride in which Cr atoms formed a fcc lattice, and the authors postulated the positions and content of H atoms. Therefore, a possible explanation for the large deviation in the lattice constant may be that the number of H atoms is less than 2 per Cr atom and/or the positions are not only the tetrahedral site. In Table V, we also indicate the results for CrH in the zinc-blende and NaCl structures, which are simple examples of fcc-based metal monohydrides. The lattice constant comes closer to the measured value in both structures, but the heat of formation in the zinc-blende structure is a moderate positive value, indicating that this phase is unstable. The heat of formation of NaCl-type CrH is nearly zero and this phase thought to be one of the candidates of the cubic chromium hydride observed experimentally. Note that the zero-point energy correction is expected to be smaller for NaCl-type CrH than for zinc-blende CrH and CaF_2-type CrH_2. More detailed investigations are required theoretically and experimentally to decide the structure and composition of the cubic chromium hydride.

TABLE V. Lattice constants a and c (Å) and heats of formation, ΔH(kJ/mol H_2), of CrH.

Structure	a	c	ΔH	
Anti-NiAs	2.685	4.368	-14	Present
	2.72	4.42		Expt.[a]
Zinc-blende	3.915	—	59	Present
NaCl	3.797	—	4	Present

[a]Reference 30.

V. SUMMARY

We have studied the $3d$ transition-metal dihydrides by the ultrasoft pseudopotential method. First, the accuracy of the theoretical prediction for hydrogenation is examined. The results for the heats of formation and heats of solution show that the calculations give the correct trends for exothermic through endothermic reactions but overbind hydrogen with transition metals, typically about 20 kJ/mol H_2. This overbinding is improved by including the zero-point energy correction. For CrH_2, a considerable difference between the calculated lattice constant and the measured one is found. In this connection, a more detailed investigation is desired.

Next, the energetics of binary dihydrides is discussed in term of three contributions: namely, the structural transformation energy, the lattice expansion energy, and the hydrogen insertion energy. The former two contributions are understood from the nature of the host metals. The hydrogen insertion energy can be represented by a simple geometric model. The extension of this model is also suitable for alloy

dihydrides. Although the predictive power of the model is still limited because of the requirement of atomic configurations in alloy dihydrides, we think that the simplicity of the model is useful for considering various effects such as alloying and substitution.

ACKNOWLEDGMENTS

We would like to thank S. Towata, M. Aoki, T. Noritake, T. Hioki, and S. Yamakawa for variable discussions. We also thank N. Ohba and N. Nagasako for their collaboration.

[1] A.R. Miedema, K.H.J. Buschow, and H.H. van Mal, J. Less-Common Met. **49**, 463 (1976); P.C.P. Bouten and A.R. Miedema, *ibid.* **71**, 147 (1980).
[2] C.D. Gelatt, H. Ehrenreich, and J.A. Weiss, Phys. Rev. B **17**, 1940 (1978).
[3] J.K. Nǿrskov, Phys. Rev. B **26**, 2875 (1982).
[4] R. Griessen, Phys. Rev. B **38**, 3690 (1988).
[5] R.C. Brouwer and R. Griessen, Phys. Rev. B **40**, 1481 (1989).
[6] M.S. Daw and M.I. Baskes, Phys. Rev. Lett. **50**, 1285 (1983).
[7] M.S. Daw and M.I. Baskes, Phys. Rev. B **29**, 6443 (1984).
[8] M.S. Daw and S.M. Foiles Phys. Rev. B **35**, 2128 (1987).
[9] H.-J. Tao, K.-M. Ho, and X.-Y. Zhu, Phys. Rev. B **34**, 8394 (1986).
[10] A. Gross, S. Wilke, and M. Scheffler, Phys. Rev. Lett. **75**, 2718 (1995).
[11] K.K. Ng, F.C. Zhang, V.I. Anisimov, and T.M. Rice, Phys. Rev. Lett. **78**, 1311 (1997).
[12] C. Elsässer, J. Zhu, S.G. Louie, M. Fähnle, and C.T. Chan, J. Phys.: Condens. Matter **10**, 5081 (1998); **10**, 5113 (1998); **10**, 5131 (1998).
[13] G.N. García, J.P. Abriata, and J.O. Sofo, Phys. Rev. B **59**, 11 746 (1999).
[14] W. Wolf and P. Herzig, J. Phys.: Condens. Matter **12**, 4535 (2000).
[15] E. Akiba and H. Iba, Intermetallics **6**, 461 (1998).
[16] D. Vanderbilt, Phys. Rev. B **41**, 7892 (1990); K. Laasonen, A. Pasquarello, R. Car, C. Lee, and D. Vanderbilt, *ibid.* **47**, 10 142 (1993).
[17] P. Hohenberg and W. Kohn, Phys. Rev. **136**, B864 (1964); W. Kohn and L.J. Sham, Phys. Rev. **140**, A1133 (1965).
[18] J.P. Perdew, K. Burke, and M. Ernzerhof, Phys. Rev. Lett. **77**, 3865 (1996); **78**, 1396(E) (1997).
[19] D.D. Koelling and B.N. Harmon, J. Phys. C **10**, 3107 (1977).
[20] A.M. Rappe, K.M. Rabe, E. Kaxiras, and J.D. Joannopoulos, Phys. Rev. B **41**, 1227 (1990).
[21] S.G. Louie, S. Froyen, and M.L. Cohen, Phys. Rev. B **26**, 1738 (1982).
[22] A. Fukumoto and K. Miwa, Phys. Rev. B **55**, 11 155 (1997).
[23] V. Eyret, J. Comput. Phys. **124**, 271 (1996).
[24] N. Ohba, K. Miwa, N. Nagasako, and A. Fukumoto, Phys. Rev. B **63**, 115207 (2001).
[25] N.D. Mermin, Phys. Rev. **137**, A1141 (1965).
[26] P.E. Blöchl, O. Jepsen, and O.K. Andersen, Phys. Rev. B **49**, 16 223 (1994).
[27] C. Kittel, *Introduction to Solid State Physics*, 6th ed. (Wiley, New York, 1986).
[28] Y. Fukai, *The Metal-Hydrogen System*, Vol. 21 of *Springer Series in Material Science* (Spinger-Verlag, Berlin, 1993).
[29] C.A. Snavely and D.A. Vaughan, J. Am. Ceram. Soc. **71**, 313 (1949).
[30] *Metal Hydrides*, edited by W.M. Mueller, J.P. Blackledge, and G.G. Libowitz (Academic Press, New York, 1968).
[31] P.H.T. Philipsen and E.J. Baerends, Phys. Rev. B **54**, 5326 (1996).
[32] K. Kunc and R.M. Martin, Phys. Rev. Lett. **48**, 406 (1982).
[33] H. Krimmel, L. Shimmele, C. Elsässer, and M. Fähnle, J. Phys.: Condens. Matter **6**, 7705 (1994): The authors use the three different potentials and the energy depends slightly on them.
[34] We have not yet examined whether the zero-point energy correction improves the underbinding for MgH_2 or not.
[35] J. Friedel, in *The Physics of Metal*, edited by J.M. Ziman (Cambridge University Press, London, 1969), Chap. 8.
[36] A. Zunger, S.-H. Wei, L.G. Ferreira and J.E. Bernard, Phys. Rev. Lett. **65**, 353 (1990).